2021 43rd Annual International Conference of the
IEEE Engineering in Medicine & Biology Society (EMBC)
Oct 31 - Nov 4, 2021. Virtual Conference

A CT reconstruction method based on constrained data fidelity range estimation

Pengxin Cao, Jun Zhao and Jianqi Sun*

Abstract— **For the CT iterative reconstruction, choosing the parameters of different regularization terms has been a difficult problem. Transforming the reconstruction problem into constrained optimization can solve this problem, but determining the constraint range and accurately solving it remains a challenge. This paper proposes a CT reconstruction method based on constrained data fidelity term, which estimates the distribution of the constraint function by Taylor expansion to determine the constraint range. We respectively use Douglas-Rachford splitting (DRS) and Projection-based primal-dual algorithm (PPD) to split the reconstruction problem and solve the data fidelity subproblem. This method can accurately estimate the constrained range of data fidelity terms to ensure reconstruction accuracy and use different regularization terms for reconstruction without parameter adjustment. Three regularization terms are used for reconstruction experiments, and simulation results show that the proposed method can converge stably, and its reconstruction quality is better than the filtered back-projection.**

I. INTRODUCTION

The optimization of the combination of the data fidelity term and regularization term is a common form of CT reconstruction methods in recent years. Plug and play(PnP) is a framework for solving this problem with split optimization algorithms such as alternating direction method of multipliers (ADMM) [1] or primal-dual splitting (PDS) [2]. The proximal operator of regularization in PnP is treated as a denoiser, and advanced regularization terms and even filters can be used for CT reconstruction.

The determination of the balance parameter for different regularization terms is a difficult problem. Some studies have proposed constrained data fidelity terms $||Ax-y||_2^2 \leq \varepsilon$. Sidky et al. [3] and Niu et al. [4] both uses constrained data fidelity term, but solve the data constraint with a back-projection method. Alfonso et al. [5] proposed an ADMM-based method to solve the constrained image restoration problem, but each iteration requires solving a large-scale linear equation system. Shunsuke Ono uses the PDS method to solve the same problem [2]. PDS does not need to solve large-scale linear equations but can only solve convex problems, and the parameters are limited to the system matrix. The meaning of ε is the noise level of data, but few studies discuss the specific method of determining ε.

This work is partly supported by National Key Research and Development Program (2016YFC01004608), National Natural Science Foundation of China (No. U1732119 and 11575115), Shanghai Jiao Tong University Medical Engineering Cross Research Funds (YG2021ZD05).

P Cao, J Zhao, and J Sun are with School of Biomedical Engineering, Shanghai Jiao Tong University, Shanghai, Co 200240 China, Corresponding email:milesun@sjtu.edu.cn

In this article, we use Douglas-Rachford splitting (DRS) [6]- a variant of ADMM - as a splitting algorithm to solve the reconstruction problem with nonconvex regularization terms. Projection based primal–dual algorithm (PPD) [7] which is similar to PDS but more robust, solves the subproblem of constrained data fidelity. The data fidelity term is regarded as a random variable function of the measurement data, and we estimate its distribution with Taylor expansion method to determine constrained rang.

II. NOISE MODEL AND DATE FIDELITY TERM

Assuming a monochromatic light source and measured by the number of photons, the measurement data is:

$$y_i = \ln \frac{N_0}{z_i} \tag{1}$$

Where N_0 represents the number of photons incident, z_i and y_i are the transmission data and sinogram data of the i-th X-ray, respectively. Using Poisson + Gaussian model [8], we have:

$$\begin{aligned} z_i &\sim Poisson(z_i^*) + Normal(0, \sigma_G^2) \\ z_i^* &= N_0 e^{-[Ax]_i} = N_0 e^{-y_i^*} \end{aligned} \tag{2}$$

Where z_i^* is the mean of z_i, σ_G^2 is the variance of Gaussian noise, and generally, Gaussian noise is much smaller than quantum noise $\sigma_G^2 \ll z_i^*$. $x \in \mathbb{R}^{N\times 1}$ is the image of linear attenuation, and $A \in \mathbb{R}^{K\times N}$ is system matrix. K and N are the numbers of projections and pixels, respectively. $y^* = Ax$ is the ideal value of y.

We define a weighted distance D from y^* to y,

$$D = \sqrt{\sum_{i=1}^{K} w_i (y_i^* - y_i)^2} \tag{3}$$

where w_i is the weight. Generally, we set w_i as the reciprocal of the variance of y_i.

Let $S = diag\{\sqrt{w_i}\}$, $A_S = SA$ and $y_S = Sy$, and then

$$\begin{aligned} D &= \sqrt{(Ax-y)^T S^T S (Ax-y)} \\ &= \|A_S x - y_S\|_2 \end{aligned} \tag{4}$$

In this article, we take the constraint of D as the data fidelity term.

Perform Taylor expansion for (1) at z_i^* and estimate the mean u_{yi} and variance σ_{yi}^2 of y_i with the expansion result [9]. When z_i^* is a large number and $z_i^* \gg \sigma_G^2$, we can get $u_{yi} = y_i^*$ $\sigma_{yi}^2 = \frac{e^{y_i^*}}{N_0} + \frac{e^{2y_i^*}\sigma_G^2}{N_0^2}$. We approximate that $\sigma_{yi}^2 = \frac{e^{y_i}}{N_0} + \frac{e^{2y_i}\sigma_G^2}{N_0^2}$.

Let $t_i = \sqrt{w_i}(y_i^* - y_i) \sim Normal(0,1)$, $D^2 = \sum_{i=1}^{K} t_i^2$. Sim-

ilarly, use Taylor expansion to estimate the distribution of D^2. When $u_{t_i}=0$, it can get $u_{D^2}=\sum_{I=1}^{k}\sigma_{t_i}^2$,$\sigma_{D^2}=2\sum_{I=1}^{k}\sigma_{t_i}^4$, and D^2 obeys the normal distribution.

$$D^2 \sim Normal\,(K,2K) \tag{5}$$

In this article, we limit the value range of D^2 to $[u_{D^2}-4\sigma_{D^2},u_{D^2}+4\sigma_{D^2}]$. With indicator function $l_C(x)$(If $x\in C$, $l_C(x)=0$, otherwise $l_C(x)=+\infty$.), CT reconstruction is expressed as a constraint optimization problem.

$$\arg\min_x l_{B_x}(x)+R(x) \tag{6}$$

Where $B_x=\{x|\,\varepsilon_1\le\|A_Sx-y_S\|_2\le\varepsilon_2\}$, $\varepsilon_1=\sqrt{K-4\sqrt{2K}}$ $\varepsilon_2=\sqrt{K+4\sqrt{2K}}$, and $R(x)$ is the regularization term.

III. OPTIMIZATION METHOD

DRS can be regarded as a fixed-point iterative algorithm and recently proved to be suitable for nonconvex problems [10] [1] [6].The suitable optimization problem form of DRS is $\arg\min_x \varphi_1(u)+\varphi_2(u)$. The DRS iterative steps for solving (6) are:

$$\begin{aligned} u_k &= prox_{pR}(s_k)\\ v_k &= prox_{pl_{B_x}}(2u_k-s_k)\\ s_{k+1} &= s_k+v_k-u_k \end{aligned} \tag{7}$$

Where p is a constant, u_k(or v_k) is the solution to the problem and $prox_{rf}$ denotes the proximity operator of function f:

$$prox_{rf}(z)=\arg\min_x f(z)+\frac{1}{2r}\|y-z\|_2^2 \tag{8}$$

$prox_{pR}(s_k)$ is equivalent to a denoising procedure for the noisy image s_k, and it can be replaced by a denoiser $\phi(s_k,p)$. p is a denoising parameter, which does not affect the final result in convex problems. Different advanced regularization or denoising models can be conveniently applied to the reconstruction problem in this step.

Let $z=2u_k-s_k$, $prox_{pl_{B_x}}(z)$ equals to the projection from z onto the set B_x, noted $P_{B_x}(z)$ and we can set p to any suitable value in this step. PPD can solve this problem.

Alotaibi et al. proposed PPD in 2015 [7], which, compared with PDS, has fewer parameter restrictions and is more robust. For the problem of the form $\arg\min_x f(x)+g(Lx)$, the solution steps are shown in Algorithm 1, where f and g are convex functions and x^* is the solution to the problem. In practice, $\tau_k=0$ is difficult to achieve, and x_k can be the solution after multiple iterations.

Set $l_{B_y}(y)$ with $B_y=\{y|\,\varepsilon_1\le\|y-y_S\|_2\le\varepsilon_2\}$, then

$$P_{B_x}(z)=\arg\min_x l_{B_y}(A_Sx)+\tfrac{1}{2p}\|x-z\|_2^2 \tag{9}$$

let $f(x)=\frac{1}{2p}\|x-z\|_2^2$, $g(y)=l_{B_y}(y)$, and $L=A_S$. $l_{B_y}(y)$ is nonconvex, but PPD can still converge if $P_{B_y}(v)$ is approximated as (10) with $T=\frac{\varepsilon_1+\varepsilon_2}{2}$.

$$P_{B_y}(v)=\begin{cases} v & v\in B_y\\ y_S+\frac{T(v-y_S)}{\|v-y_S\|_2} & v\notin B_y \end{cases} \tag{10}$$

Algorithm 1 Projection based primal–dual algorithm (PPD)

set $r_1,r_2\in(0,+\infty)$ $\lambda_k\in(0,2)$ $x_1$and v_1 as initial

for $k=1,2\ldots$

$a_k=prox_{r_1f}(x_k-r_1L^Tv_k)$

$l_k=La_k$

$b_k=prox_{r_2g}(l_k+r_2v_k)$

$s_k=r_1^{-1}(x_k-a_k)+r_2^{-1}(l_k-b_k)$

$t_k=b_k-La_k$

$\tau_k=\|s_k\|^2+\|t_k\|^2$

if $\tau_k=0$

$x^*=a_k$

$v^*=v^*+r_2^{-1}(l_k-b_k)$

break

end

if $\tau_k\neq 0$

$\theta_k=\lambda_k(r_1^{-1}\|x_k-a_k\|^2+r_2^{-1}\|l_k-b_k\|^2)/\tau_k$

$x_{k+1}=x_k-\theta_ks_k$

$v_{k+1}=v_k-\theta_kt_k$

end

end and *return* x_{k+1}

IV. SIMULATION

The digital simulation model used in the experiment is the forbild head phantom, as shown in Fig.5 (a) , with the size 512×512. The measurement data is Uniform sampled at 512 views between 0 to 180 degrees with a detector with 640 bins. Noise is added with the model in section II, where $N_0=3000$. The convergence of PPD, the verification of ε, and the reconstruction experiment with regularization terms of TV [11], L0TV [12] and BM3D [13] are performed in simulation.

A. Convergence analysis of PPD

The four parameters, namely p, r_1, r_2 and λ need to be determined in algorithm 1 for problem $P_{B_x}(x_{ini})=\arg\min_x l_{B_y}(A_Sx)+\frac{1}{2p}\|x-x_{ini}\|_2^2$, Select the estimated range in section II as $\varepsilon_1=401.9$ $\varepsilon_2=407.6$ and set $x_{ini}=\mathbf{0}$. The experiments are performed with the parameters p, r_1, r_2, λ as [2,5,1,1], [2,1,5,1], [2,5,5,1], [20,1,1,1], [0.5,1,1,1], [2,1,1,0.5], [2,5,1,1.75], respectively.

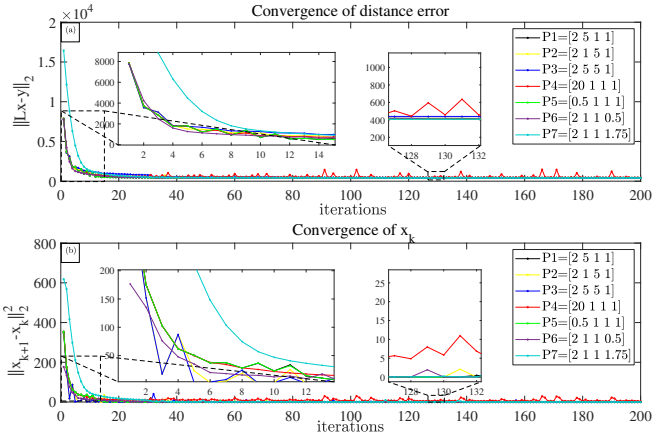

Fig. 1. Convergence curve of the result. The above is the curve of distance error, and the below is the distance of adjacent iteration points.

Fig.1(a) (b) are the curves of $\|A_sx_k-y_S\|_2$ and $\|x_{k+1}-x_k\|_2$ in the iterative process, respectively. The convergence curves drop rapidly in the first 15 iterations and then gradually reach the convergence result. The curves are very similar, and only P4 and P7 are somewhat different. P4 shows that a larger p will make the convergence unstable;

According to the result of P7, for an λ close to 2, the curve will only slowly converge in the first few iterations. Different parameters have little effect on the convergence speed of PPD. When x_{ini} is at $\{x|\,\|A_S x - y_S\|_2 < \varepsilon_1\}$, x_1 will be at $\{x|\,\|A_S x - y_S\|_2 > \varepsilon_2\}$ after the first iteration, and it will still converge to B_y. The above shows that PPD has good robustness and convergence speed.

B. Validation of parameter ε selection

To validate whether the estimated constraint range is appropriate, solve the projections of different B_x from three starting points, namely the origin(O1), a random point(O2), and FBP reconstruction results of noise-free data(O3). Set different constraint ranges as $\varepsilon_i^k = 20k + \varepsilon_i^{est}$ $k = -10, -9 \ldots 40, i = 1, 2(\varepsilon_i^{est} is$ the estimated value). Take $T_k = \frac{\varepsilon_1^k + \varepsilon_2^k}{2}$ and signal-to-noise ratio (SNR) as coordinate and evaluation index, respectively.

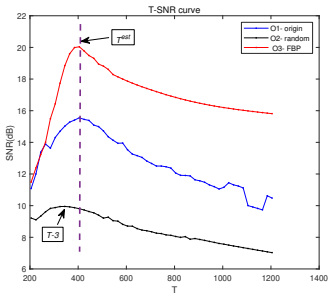

Fig. 2. The T-SNR curve of the result

Fig.2 shows the resulting T-SNR curve. The results of O1 and O3 both achieve the maximum value at T^{est}, and O2 achieves the maximum value at T_{-3}, but it is not much different from the result at T^{est} (SNR_{-3}=9.95dB,SNR_0=9.81dB). The starting point makes the curves differ greatly, and the starting point of O3 is closest to the true value while the starting point of O2 is background noise.

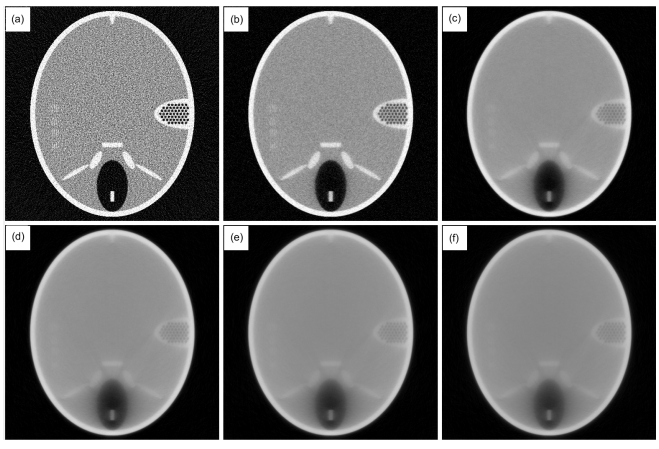

Fig. 3. Reconstructed image of zero under different constraints. (a)T_{-10}, (b) T^{est}, (c) T_{10}, (d) T_{20}, (e) T_{30}, (f) T_{40}

Fig.3 shows the result image of O1. As the value of T decreases, the image gradually changes from blurry to clear (from Fig.3(f) to (b)), and Fig.3(b) shows the image at T^{est}, which has the best quality. But as T continues to decrease, the image appears a lot of noise(In Fig.3, (a) has more noise than (b)). And in the curve in Fig.2, O2 and O3 have similar SNR at $T < 300$. When the constraint range is too close to y, each x contains the noise in y and the reconstruction accuracy is low.At this time, the regularization term cannot denoise the reconstructed image either. The above results indicate that the estimation result in Section II is the optimal value.

C. Reconstruction result

Use TV, L0TV, BM3D for image reconstruction, and set data fidelity term as described in Section II. Select appropriate regularization term denoising parameters and set the parameters as $r_{TV} = 1/15$, $r_{L0TV} = 0.01$, $\sigma_{BM3D} = 20$. The DRS method iterates 50 times for reconstruction, sets the initial point s_1 as a point in B_x, and, for fast calculation, sets the maximum number of iterations of the PPD to 50.

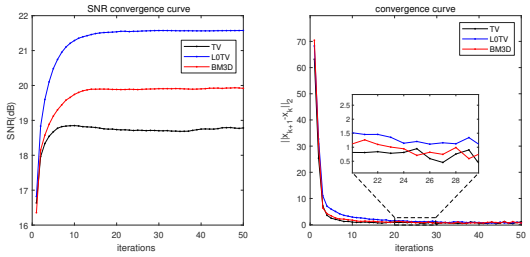

Fig. 4. Iterative convergence analysis. (a) is the SNR curve, (b) is the distance curve of adjacent iteration points.

Fig.4 shows the convergence curves of the three reconstruction methods. All three methods can converge in about 15 iterations, and the convergence speed is similar. The three regularization terms are the convex regularization term, nonconvex regularization term, and locally similar filtering operation, respectively. The results show that the algorithm can converge stably for different types of regularization terms. The step size has a specific influence on the reconstruction result for the nonconvex regularization term. If the step size is within a certain range in the experiment, L0TV will converge to the same point. In large difference in step size, L0TV will have different convergence results, but the two results are very similar.

Fig.5 is the reconstructed image, and FBP reconstructed image as a comparison. The FBP reconstructed image contains a lot of noise, and the other three reconstruction methods have different effects. Bx is the initial point s_1 of reconstruction(In other words, Bx is the reconstruction image without regularization). L0TV can retain the edges, but the small structure may disappear; TV makes the overall image smooth, not suitable for this image than L0TV. BM3D can maintain a clear structure, but there is noise in flat areas. The result of Bx is closer to the real ground than FBP. L0TV tends to "smooth" the image, that is to make less gradient changes. Therefore, in L0TV result, the flat area has less noise, but the point structure on the left is removed. But if there is enough sampling angle and number of incident electrons, it can still be reconstructed.

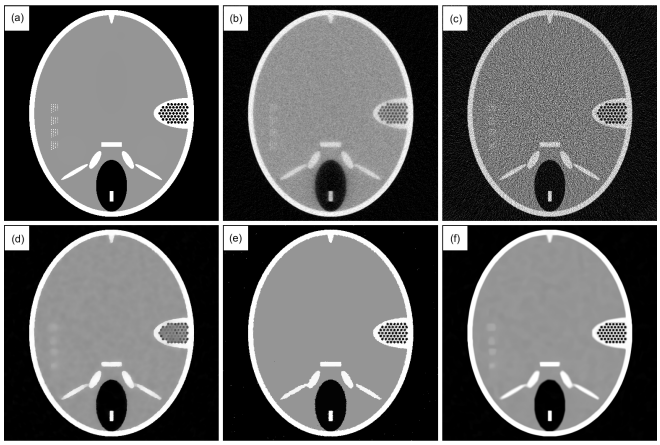

Fig. 5. Experimental reconstruction results. The reconstruction methods are (a)ground true (b)Bx (c)FBP (d)TV, (e)L0TV, (f)BM3D respectively. the display window is [0,1.8]

TABLE I
EVALUATION OF RECONSTRUCTION RESULTS

	SNR(dB)	SSIM
FBP	6.9143	0.2486
Bx	15.5425	0.5653
TV	18.7735	0.9026
L0TV	21.5757	0.9556
BM3D	19.9181	0.9169

Table I shows the evaluation of the reconstruction results by SNR and SSIM. The index of Bx is significantly better than FBP, which indicates the accuracy of the solution in the data fidelity constraint set.The indicators of TV, L0TV, and BM3D are better than Bx, and the regularization term can further improve the reconstruction quality. The performance of TV, L0TV, and BM3D are different, and the choice of regularization term depends on the nature of the reconstructed image.

V. CONCLUSIONS AND DISCUSSION

This paper proposes a method for estimating the range of constrained data fidelity term and solve the reconstruction problem with DRS and PPD. Regarding the constraint function as a function of the random variable of the measurement data, estimate the distribution of constraint function with the second-order Taylor expansion, and determine the constraint range of the constraint according to the distribution. The DRS method decomposes the reconstruction problem, and the data fidelity term and regularization term are in different subproblems. PPD is used to solve the subproblem of data fidelity term, and different regularization terms can be flexibly combined with the proposed reconstruction method. The three regularization terms TV, L0TV, and BM3D are used for reconstruction simulation. The results show that the reconstruction quality of the three regularizations is better than FBP with SNR and SSIM as indicators. The advantage of this method is that different regularization terms can be easily applied for reconstruction, and the parameter can be determined only by the number of incident photons and scanning information.

The data fidelity term adopts a weighted form to balance the difference in noise level between X-rays. According to the distribution estimation of D, two thresholds of the constraint are determined. Each solution in the constraint is very likely to be close to the true value, thus ensuring the lowest reconstruction accuracy.

Three regularization terms with different properties are used in reconstruction experiments to verify convergence. The regularization term represents the prior knowledge of the image, and for a certain data fidelity term, it determines the reconstruction result. In theory, for nonconvex regularization terms, the step size also affects the reconstruction results. In practice, due to the constrained data fidelity term, the reconstruction results of the same regularization term with different step sizes are similar. For a regularization term, especially in nonconvex, choosing the best step size, that is, to achieve global convergence, still needs further research.

REFERENCES

[1] Y. Wang, W. Yin, and J. Zeng, "Global convergence of admm in nonconvex nonsmooth optimization," *Journal of Scientific Computing*, vol. 78, no. 1, pp. 29–63, 2019.

[2] S. Ono, "Primal-dual plug-and-play image restoration," *IEEE Signal Processing Letters*, vol. 24, no. 8, pp. 1108–1112, 2017.

[3] E. Y. Sidky, C.-M. Kao, and X. Pan, "Accurate image reconstruction from few-views and limited-angle data in divergent-beam ct," *Journal of X-ray Science and Technology*, vol. 14, no. 2, pp. 119–139, 2006.

[4] T. Niu and L. Zhu, "Accelerated barrier optimization compressed sensing (abocs) reconstruction for cone-beam ct: Phantom studies," *Medical physics*, vol. 39, no. 7Part2, pp. 4588–4598, 2012.

[5] M. V. Afonso, J. M. Bioucas-Dias, and M. A. Figueiredo, "An augmented lagrangian approach to the constrained optimization formulation of imaging inverse problems," *IEEE Transactions on Image Processing*, vol. 20, no. 3, pp. 681–695, 2010.

[6] W. Ouyang, Y. Peng, Y. Yao, J. Zhang, and B. Deng, "Anderson acceleration for nonconvex admm based on douglas-rachford splitting," in *Computer Graphics Forum*, vol. 39, pp. 221–239, Wiley Online Library, 2020.

[7] A. Alotaibi, P. L. Combettes, and N. Shahzad, "Solving coupled composite monotone inclusions by successive fejer approximations of their kuhn–tucker set," *SIAM Journal on Optimization*, vol. 24, no. 4, pp. 2076–2095, 2014.

[8] L. Fu, T.-C. Lee, S. M. Kim, A. M. Alessio, P. E. Kinahan, Z. Chang, K. Sauer, M. K. Kalra, and B. De Man, "Comparison between pre-log and post-log statistical models in ultra-low-dose ct reconstruction," *IEEE transactions on medical imaging*, vol. 36, no. 3, pp. 707–720, 2016.

[9] J. Ma, Z. Liang, Y. Fan, Y. Liu, J. Huang, W. Chen, and H. Lu, "Variance analysis of x-ray ct sinograms in the presence of electronic noise background," *Medical physics*, vol. 39, no. 7Part1, pp. 4051–4065, 2012.

[10] M. L. Gonçalves, J. G. Melo, and R. D. Monteiro, "Convergence rate bounds for a proximal admm with over-relaxation stepsize parameter for solving nonconvex linearly constrained problems," *arXiv preprint arXiv:1702.01850*, 2017.

[11] Y. Dong, M. Hintermüller, and M. Neri, "An efficient primal-dual method for l^1 tv image restoration," *SIAM Journal on Imaging Sciences*, vol. 2, no. 4, pp. 1168–1189, 2009.

[12] L. Xu, C. Lu, Y. Xu, and J. Jia, "Image smoothing via l 0 gradient minimization," in *Proceedings of the 2011 SIGGRAPH Asia Conference*, pp. 1–12, 2011.

[13] K. Dabov, A. Foi, V. Katkovnik, and K. Egiazarian, "Image denoising by sparse 3-d transform-domain collaborative filtering," *IEEE Transactions on image processing*, vol. 16, no. 8, pp. 2080–2095, 2007.